electronics

MDPI

Article

On the Use of Near-Field Constellation Focusing for Physical Layer Security with Extremely Large Antenna Arrays

João Ferreira [1,2,*], João Guerreiro [1,2], Rui Dinis [1,2,*] and Paulo Montezuma [1,2,3,*]

[1] NOVA School of Science and Technology, 2829-516 Caparica, Portugal; jf.guerreiro@fct.unl.pt
[2] Instituto de Telecomunicações, 3810-193 Aveiro, Portugal
[3] Uninova—Instituto de Desenvolvimento de Novas Tecnologias, Quinta da Torre, 2829-517 Caparica, Portugal
* Correspondence: jpsr.ferreira@campus.fct.unl.pt (J.F.); rdinis@fct.unl.pt (R.D.); pmc@fct.unl.pt (P.M.)

Abstract: In the fast-changing world of wireless communications, the combination of extremely large antenna arrays (ELAAs) and energy-efficient transmission methods is envisioned for the 6G. The application of directivity in the transmitted constellation can increase physical layer security (PLS) and promote the energy efficiency of transmission. In such scenarios, large constellations can be divided into multiple binary phase shift keying (BPSK) components, with each component being individually amplified and transmitted by an antenna. In this work, we consider an ELAA acting as a transmitter and constellation decomposition at the sub-array level. We investigate the impact of considering a near-field channel model in terms of secrecy rate and mutual information. In addition to the energy efficiency of the constellation decomposition, it is demonstrated that the particularities of near-field beamforming increase the PLS, namely in terms of robustness to eavesdropping.

Keywords: near field; physical layer security; directivity; optimized constellations

Citation: Ferreira, J.; Guerreiro, J.; Dinis, R.; Montezuma, P. On the Use of Near-Field Constellation Focusing for Physical Layer Security with Extremely Large Antenna Arrays. *Electronics* **2024**, *13*, 869. https://doi.org/ 10.3390/electronics13050869

Academic Editors: Yan Zhang, Sye Loong Keoh and Minghui Li

Received: 20 December 2023
Revised: 9 February 2024
Accepted: 21 February 2024
Published: 23 February 2024

1. Introduction

The broadcast nature of wireless channels gives rise to a significant concern regarding security in wireless communication systems. Typically, security is ensured through encryption algorithms implemented in higher layers of the Open Systems Interconnection (OSI) stack, such as key cryptography protocols [1]. The inherent broadcast nature of wireless communications poses challenges in preventing the unauthorized interception of transmitted signals, and the phenomenon of superposition can result in the overlap of multiple signals at the receiver [2]. Nevertheless, security can be augmented with alternative approaches, such as physical layer security (PLS) schemes [3]. Given their independence from higher layers, PLS techniques can be employed on top of existing security schemes. Common techniques in PLS involve the use of coding or precoding schemes and leverage channel state information to maintain confidentiality across a wireless medium [4].

Multiple-input, multiple-output (MIMO) systems offer extensive spatial multiplexing capabilities due to their impressive ability to filter signals in the spatial domain, demonstrating high spatial selectivity. Indeed, MIMO arrays can efficiently transmit and/or receive signals in a specific direction and with very narrow beamwidth [5]. Consequently, the array gain experiences a rapid decrease outside the receive/transmit direction, which promotes PLS. Among the various PLS techniques proposed for sixth generation (6G), the utilization of large antenna systems stands out as one of the most promising approaches, particularly through the application of narrow beamforming facilitated by extremely large antenna array (ELAA) [6]. The huge aperture of ELAAs and/or the adoption of higher carrier frequencies gives rise to a larger near-field region. As a result, the communication channels to/with ELAAs should consider spherical wave propagation, and cannot rely on the far-field plane-wave channel modeling of conventional MIMO. Recent findings have demonstrated that beamforming in the near field not only produces narrow beams but

also results in beams with finite depth. This is fundamentally different from the conventional beamforming associated with the far-field region, which is characterized by infinite depth [7–9]. Therefore, an ELAA can potentially concentrate its large gain in a specific zone, which gives rise to a beamfocusing effect [9,10]. This effect can be used to increase PLS features [11–13].

Spectrally efficient wireless communications are based on single-carrier multilevel Quadrature Amplitude Modulation (QAM) constellations and/or on multicarrier signals. In both cases, the transmitted signals exhibit a large peak-to-average power ratio (PAPR) and lead to amplification issues because the power amplifier must adopt a large input back-off to avoid nonlinear distortion [14]. A solution to this problem is to employ a parallel amplification technique with constellation decomposition [15]. In this technique, multi-level constellations are divided into multiple Binary Phase Shift Keying (BPSK), Quadrature Phase Shift Keying (QPSK), or Offset Quadrature Phase Shift Keying (OQPSK) components, and each component is individually amplified and transmitted by an antenna. The different components are combined at the channel level to generate the desired data symbols. Phase rotations between Radio Frequency (RF) branches can be selected to optimize the transmitted constellation in a specific direction. Consequently, PLS is achieved through the shaping of the constellation, which ensures that unauthorized users cannot decode the data transmitted to the legitimate user [16,17].

1.1. Related Work

In recent years, extensive research has focused on the PLS features within MIMO systems. As detailed in [18], various techniques have been proposed to enhance PLS in massive MIMO, including artificial noise [19], deep learning [20], and power allocation [21]. Those works share the plane-wave assumption for channel modeling. However, increasing focus on near-field communications, particularly in the context of large antenna arrays for 6G, has prompted the need for channel models that account for spherical wave propagation. The PLS gains associated with near-field beamforming were firstly addressed in [22], where authors focus on spatial domain characteristics in extra-large scale MIMO (XL-MIMO) systems. Their study emphasized the impact of near-field beamforming on PLS, particularly in conjunction with the spherical-wavefront model. In [11,12], the authors considered the PLS features in radiative near-field communication for ELAAs, demonstrating that beamfocusing with Matched Filtering (MF) beamforming substantially improves jamming rejection and secrecy rates. In [16], the focus lies on achieving PLS through constellation shaping. Note the proposed approach necessitates each user's knowledge of the transmitter configuration parameters related to constellation shaping. In [17], the authors proposed a PLS approach that combines constellation shaping with a MIMO transmission in the plane-wave regime.

Table 1 summarizes the related work described above, highlighting the underlying PLS technique and the main differences relatively to the proposed PLS scheme.

Table 1. Main relevant work and their principal differences relative to the proposed PLS scheme.

Reference	PLS Technique	Key Differences
[11,12]	MF beamfocusing.	Does not use constellation decomposition techniques.
[17]	Constellation decomposition.	Far-field communications and plane-wave approximation.
[19]	Artificial noise.	Far-field communications and plane-wave approximation.
[20]	Deep learning.	Far-field communications and plane-wave approximation.
[21]	Power allocation.	Far-field communications and plane-wave approximation.
[22]	MF beamforming.	Does not use constellation decomposition techniques.

1.2. Major Contributions

This paper considers a novel transmission scheme where an ELAA is combined with a multi-level QAM decomposition technique to provide energy-efficient and secure downlink transmissions. The major contributions are summarized as follows:

- Contrary to the approach of [17], which considered a MIMO system operating in the far field and a group of antennas to transmit each constellation component, we considered constellation decomposition at the ELAA level, and that each component is transmitted by an individual sub-array operating in the near-field.
- We consider a near-field channel model for each sub-array and compare its particularities relative to a common far-field channel model.
- We studied the PLS aspects resulting from the combination of near-field beamforming and constellation shaping, namely by analyzing the achievable mutual information (MI) and secrecy rate (SR) under various scenarios.

By investigating factors such as field region, relative distance, beamforming direction, and the transmitted constellation configuration, this work aims to provide insights into how the integration of these techniques contributes to improved SR and MI. It is demonstrated that in the near-field, the PLS features of the QAM constellation decomposition scheme can be better than the ones observed in the far field, which is explained by the beamfocusing effect available in this field region

1.3. Organization

This work is structured into distinct sections: Section 2 provides details on the adopted communication scenario under consideration. It also delves into channel modeling within the near field. Section 3 describes the decomposition of the M-QAM constellation and also presents the PLS features of this decomposition technique achieved both in the far field and in the near field. Lastly, Section 4 outlines the conclusions drawn from this work.

1.4. Notation

The notation used in this context is as follows: Boldface lowercase letters stand for vectors, and the nth element of a vector is denoted as $\mathbf{x}_n$ The norm of $\mathbf{v}$ is denoted as $||\mathbf{v}||$, and $\hat{\mathbf{v}} = \frac{\mathbf{v}}{||\mathbf{v}||}$ represents the direction of $\mathbf{v}$. The symbol $(\cdot)^H$ represents the Hermitian operator, which is equivalent to the transpose conjugate. The function $\text{mod}(a, b)$ yields the remainder of the integer division $\frac{b}{a}$, the division operation, denoted as $a \div b$, yields the quotient when a is divided by b, and $\lfloor \cdot \rfloor$ represents the floor function. The imaginary unit is denoted as $\text{j} = \sqrt{-1}$.

2. System Characterization

2.1. Communication Scenario

In this work, it is considered a single carrier (SC) transmission between an ELAA, a legitimate user, and a malicious user posing as an eavesdropper, both equipped with single isotropic antennas. This transmission occurs in a line of sight (LoS) channel on the carrier frequency f_c, where $\lambda = \frac{c}{f_c}$ represents the wavelength and c is the speed of light. Unless otherwise stated, we adopt a carrier frequency $f_c = 3$ GHz.

As illustrated in Figure 1, the ELAA is deployed in the YZ plane. Moreover, the ELAA is divided into K sub-arrays with Q non-contiguous antennas, each of which spaced by $\lambda/2$. The total number of antennas is $N = K \times Q$. Also, the total number of antennas can be calculated using $N = N_h \times N_v$, where N_h denotes the number of antennas along the y-axis (i.e., along the array's horizontal dimension) and N_v indicates the number of antennas along the z-axis (i.e., along the array's vertical dimension). To provide a more detailed explanation of the ELAA antenna geometry, let us focus on N_h. In this context, this variable can be further decomposed into $N_h = K \times P$, where P is the horizontal dimension of each sub-array. Moreover, the vertical dimension of each sub-array is N_v. Consequently, we can express the total number of antennas of a sub-array as $Q = P \times N_v$. Therefore, the total

number of antennas of the ELAA is also given by $N = K \times P \times N_v$. The index of a given sub-array is given by $k = \text{mod}(n_v n_h - 1, K) + 1$.

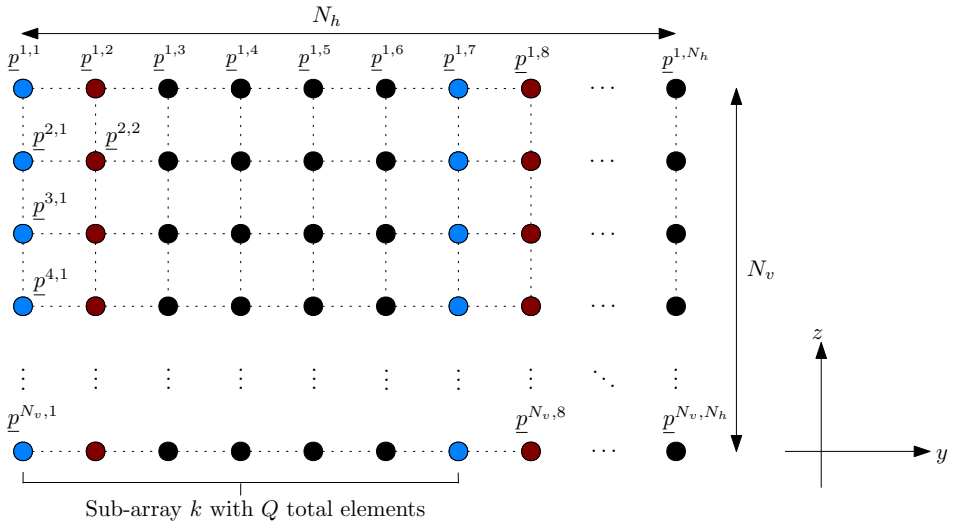

Figure 1. Considered ELAA deployed on the YZ plane.

The antenna positions within the ELAA are denoted by $\underline{p}^{n_v,n_h} = (0, y_{n_h}, z_{n_v})$. The upper index identifies the antenna position within the ELAA, whilst the sub-index k indicates the sub-array the antenna (n_v, n_h) pertains to. The coordinates of a given antenna can be calculated by

$$\begin{cases} y_{n_h} & = -\frac{\lambda}{4}(N_h - 1) + \frac{\lambda}{2}\text{mod}(n_h - 1, N) \\ z_{n_v} & = \frac{\lambda}{4}(N_v - 1) + \frac{\lambda}{2}\text{mod}(n_v - 1, N) \end{cases}. \tag{1}$$

The positions of the legitimate and malicious users are defined by $\underline{p_l} = (x_l, y_l, z_l)$ and $\underline{p_m} = (x_m, y_m, z_m)$, respectively. Since both users are situated in the XY plane (i.e., $z_l = z_m = 0$), the z axis coordinate is disregarded when defining their locations. Also, an alternative polar definition for these positions can be considered. Concretely, $\underline{p_l} = (x_l, y_l) = (d_l \sin(\theta_l), d_l \cos(\theta_l))$ and $\underline{p_m} = (x_m, y_m) = (d_m \sin(\theta_m), d_m \cos(\theta_m))$, where d_l and d_m represent the distance between the user and the center of the ELAA and θ_l and θ_m are the users' directions relatively to the ELAA. Note also that $d_m = d_l + \Delta d$ and $\theta_m = \theta_l + \Delta\theta$, where Δd and $\Delta\theta$ are the distance and angular deviations of the malicious user. Note that d, d_l, and Δ_d are measured in meters and all angles are expressed in degrees A top view of the considered communication scenario is illustrated in Figure 2.

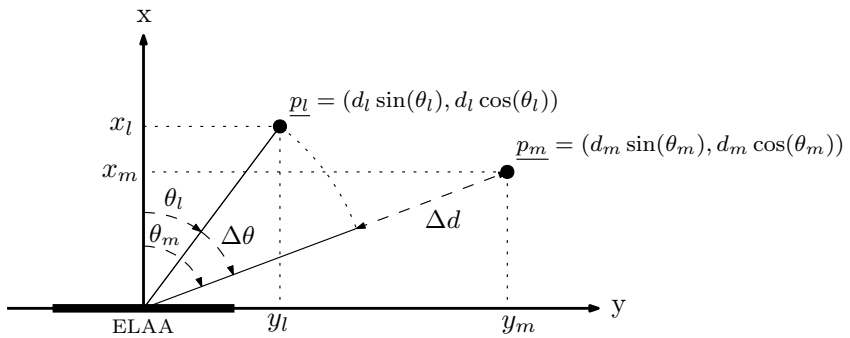

Figure 2. Top view of the considered communication scenario with an ELAA transmitting to a legitimate user and a malicious eavesdropper.

2.2. Near-Field Channel Modeling

When dealing with ELAAs, accurately modeling the underlying propagation characteristics of the communication link becomes crucial. This necessity arises from the

substantial increase in the far-field distance, implying a heightened likelihood that the communication occurs in the near field. Despite the propagation distance potentially exceeding the Fraunhofer distance of each antenna element, it is important to note that the distance might remain considerably lower than the Fraunhofer array distance, which is defined as $\mathcal{D}_{FA} = \frac{2D_{\text{sub}}^2}{\lambda}$, where D_{sub} is the maximum distance between antennas of a given sub-array [11].

Let us consider a user at a generic position $\underline{p} = (x, y, z)$ communicating with an antenna of the ELAA situated at $\underline{p}^{n_v,n_h} = (0, y_{n_h}, z_{n_v})$. The propagation distance of this communication link can be calculated by

$$d(\underline{p}^{n_v,n_h}, \underline{p}) = \sqrt{x^2 + (y_{n_h} - y)^2 + (z_{n_v} - z)^2}. \tag{2}$$

Given the effective distances between the two points in space, the effective channel response between a user located at $\underline{p} = (x, y)$ and the antenna of the ELAA at $\underline{p}^{n_v,n_h}$ can be computed as

$$\begin{aligned} h_{n_v,n_h} &= \frac{\lambda}{4\pi d(\underline{p}^{n_v,n_h}, \underline{p})} e^{-j\frac{2\pi}{\lambda} d(\underline{p}^{n_v,n_h}, \underline{p})}, \\ &= \frac{\lambda}{4\pi\sqrt{x^2 + (y_{n_h} - y)^2 + (z_{n_v} - z)^2}} e^{-j\frac{2\pi}{\lambda}\sqrt{x^2+(y_{n_h}-y)^2+(z_{n_v}-z)^2}}. \end{aligned} \tag{3}$$

We consider a transmission scheme where each sub-array transmits a different signal to the legitimate user so that a total number of K different signals are transmitted. The channel associated to the kth sub-array is defined as $\mathbf{h}^{(k)} = [h_1^{(k)}\ h_2^{(k)}\ ...\ h_Q^{(k)}]^T$. Note that the q$th$ antenna index of the sub-array K can be translated into an index (n_v, n_h) index in the ELAA where $n_v = \text{mod}(q, N_v)$ and $n_h = (q \div N_v)K + 1$.

For beamforming at each sub-array, we consider the MF criteria. Therefore, the beamforming weights for the kth sub-array are defined as

$$\mathbf{w}^{(k)} = \frac{\mathbf{h}^{(k)}}{||\mathbf{h}^{(k)}||}, \tag{4}$$

where $||\mathbf{w}^{(k)}||^2 = 1$. It is important to note that if a user is situated in the far field, conventional beamforming based on angle-of-arrival (AoA) can replace the beamforming weights derived from the user's position. However, in the near-field scenario, the beamforming weights must be precisely defined based on the effective positions of the users.

3. Constellation Decomposition Using Antenna Arrays

One approach to increase the spectral efficiency of communication systems is to use large QAM constellations. However, multilevel QAM constellations lead to amplification issues, thanks to the resulting high PAPR. These issues are due to the need to adopt a high input back-off (IBO) to assure a linear amplification of the transmitted signal, which strongly reduces the power efficiency of the power amplifier (PA) [23]. In this section, we follow a strategy to increase the power efficiency of the communication based on the one proposed in [17]. The main idea is to decompose the large-PAPR signal into a set of constant-envelope signals such as BPSK or QPSK signals. Each signal is transmitted by a strongly nonlinear, energy-efficient PA [24]. In this work, we consider a decomposition with BPSK components, since in this case, we have more spatial degrees of freedom to focus the constellation.

Let us consider 64-QAM constellations, which can be decomposed into $K = \log_2(M) = 6$ BPSK components. Each BPSK component is transmitted individually using an arbitrary antenna structure (as will be clarified later in the manuscript, each BPSK component can be transmitted by a single antenna or by a large sub-array). The data bits are mapped into the

64-QAM constellation, characterized by the ordered set $\mathfrak{S} = \{s_0, s_1, \ldots, s_{M-1}\}$ following the rule $\left(\beta_n^{(\mu-1)}, \beta_n^{(\mu-2)}, \ldots, \beta_n^{(1)}, \beta_n^{(0)}\right) \mapsto s_n \in \mathfrak{S}$, with $\left(\beta_n^{(\mu-1)}, \beta_n^{(\mu-2)}, \ldots, \beta_n^{(1)}, \beta_n^{(0)}\right)$ denoting the binary representation (i.e., 0 or 1) of s_n with $\mu = \log_2(M)$ bits. The decomposition rule for the particular case of 64-QAM can be obtained as [17], where

$$s_n = g_1 b_n^{(1)} + g_2 b_n^{(1)} b_n^{(2)} + g_3 b_n^{(1)} b_n^{(2)} b_n^{(3)} + g_4 b_n^{(4)} + g_5 b_n^{(4)} b_n^{(5)} + g_6 b_n^{(4)} b_n^{(5)} b_n^{(6)}, \quad (5)$$

with $\left(b_n^{(\mu-1)}, b_n^{(\mu-2)}, \ldots, b_n^{(1)}, b_n^{(0)}\right)$ denoting the binary polar representation (i.e., ± 1) of the symbol s_n and $g_1 = 1$, $g_2 = j$, $g_3 = 2$, $g_4 = 2j$, $g_5 = 4$ and $g_6 = 4j$. For the considered 64-QAM constellation, the different BPSK components are defined in Table 2.

Table 2. Definition of the $K = 6$ BPSK components of the considered 64-QAM constellation.

k	**BPSK Component**	**Possible Values**
1	$g_1 b_n^{(1)}$	± 1
2	$g_2 b_n^{(1)} b_n^{(2)}$	$\pm j$
3	$g_3 b_n^{(1)} b_n^{(2)} b_n^{(3)}$	± 2
4	$g_4 b_n^{(4)}$	$\pm 2j$
5	$g_5 b_n^{(4)} b_n^{(5)}$	± 4
6	$g_6 b_n^{(4)} b_n^{(5)} b_n^{(6)}$	$\pm 4j$

As can be observed, each of the BPSK components can be transmitted efficiently using a nonlinear PA, given that we are employing BPSK modulation, which maintains a constant envelope, allowing for the use of nonlinear and efficient PAs without experiencing Non-Linear (NL) distortion. It should also be highlighted that a given receiver (either the legitimate user or the eavesdropper) receives a complex data symbol $\tilde{s}_n$ that results from the combination of all the BPSK components in the channel. Naturally, since the different signals are precoded to combine coherently at the location of the legitimate user, PLS features can be explored with this transmission scheme since an eavesdropper located at a different position has difficulties decoding the received constellation.

To analyze and evaluate the PLS benefits of the constellation decomposition technique, we consider the SR between the legitimate user and the eavesdropper. The MI for the combined symbol is denoted by $\tilde{s}_n$ and can be calculated as [17]

$$I(\tilde{s}_n) = \log_2 M - \frac{1}{M} \sum_{\tilde{s}_n \in \mathfrak{S}} \mathbf{E}_n \left[\log_2 \left(\sum_{\tilde{s}'_n \in \mathfrak{S}} \exp\left(-\frac{1}{N_0} \left| (\tilde{s}_n - \tilde{s}'_n) + \nu \right|^2 - |\nu|^2 \right) \right) \right], \quad (6)$$

where $\mathbf{E}_n$ represents the expected value, ν represents the noise, N_0 stands for the noise power spectral density, and $\tilde{s}'_n$ represents the symbol of the original 64-QAM. The SR is defined as the difference between the MIs of the legitimate and malicious user, i.e.,

$$\mathrm{SR} = I_l(\tilde{s}_n) - I_m(\tilde{s}_n), \quad (7)$$

where I_l represents MI of the legitimate user and I_m represents the MI of the eavesdropper.

In the next subsections, we present an analysis of the PLS features of this decomposition technique considering both the transmission with a uniform linear array (ULA) with K antenna elements (Section 3.1) and an ELAA with K sub-arrays with arbitrary dimensions (Section 3.2).

3.1. Transmission with ULAs

A ULA is a type of antenna array configuration where the antennas are arranged in a straight line with equal spacing between adjacent antennas. In this section, we consider an ULA with $K = 6$ antennas to transmit the BPSK components of a 64-QAM constellation defined in Table 2. The considered ULA is represented in Figure 3.

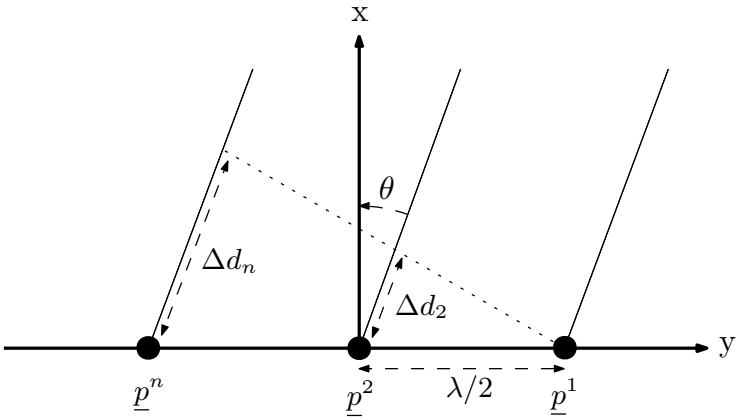

Figure 3. Considered ULA geometry with signals being transmitted with an angle-of-departure θ.

This ULA can be seen as a particular case of the general antenna array characterized in Section 2, with $Q = 1$ and $K = 6$, which results in $P = N_h = 1$ and $N_v = K$, yielding a total of $N = 6$ antennas. Note that since the ULA is physically small, it is very likely that both the legitimate user and the eavesdropper are located in the far-field region. As a result, channel modeling can be simplified thanks to the fact that the phase variations across the antennas of the ULA can be defined as a function of the angle-of-departure (AoD) θ (see Figure 3). More concretely, the complex-valued channel response of the kth antenna can be written as

$$\begin{aligned} h^{(k)} &= \frac{\lambda}{4\pi d} e^{-j\frac{2\pi}{\lambda}\Delta d_n}, \\ &= \frac{\lambda}{4\pi d} e^{-j\pi(k-1)\sin\theta}. \end{aligned} \tag{8}$$

Each BPSK component is transmitted to the legitimate user using MF beamforming. In this context, the beamforming weights for the kth sub-array are defined as

$$w^{(k)} = e^{j\pi(k-1)\sin\theta}. \tag{9}$$

Under these conditions, the received complex data symbol is

$$\tilde{s}_n = \sum_{k=1}^{K} s_n^{(k)} w^{(k)} h^{(k)}. \tag{10}$$

Let us now evaluate the PLS performance of this technique. More concretely, we present a set of results regarding the MI and the SR computed using Equations (6) and (7). Rate formulas are presented as a function of $\frac{E_b}{N_0}$, where $\frac{N_0}{2}$ represents the noise variance, and E_b corresponds to the average energy of the transmitted bits. It is assumed that the transmitter employs linear power amplification, and also a perfect time and frequency synchronization. Let us start by considering a scenario where the legitimate user at a distance $d_l = d_{FA}$ (i.e., in the far-field region of the ULA), whilst the malicious user is at $d_m = d_l + \Delta d$ with $\Delta d = 25\lambda$. Both users are located at the array's boresight, $\theta_m = \theta_l = 0^\circ$ (i.e., $\Delta\theta = 0^\circ$).

As it can be noted from Figure 4, both legitimate and eavesdropper MI follow the same behavior and saturate at 6 bits/s/Hz. As a consequence, the SR remains close to

zero as both MI values increase equally with the signal-to-noise ratio (SNR). Both users experience similar normalized beamforming gain as both are in the far field and similar constellation shapes as there is no angular difference between both users ($\Delta\theta = 0°$).

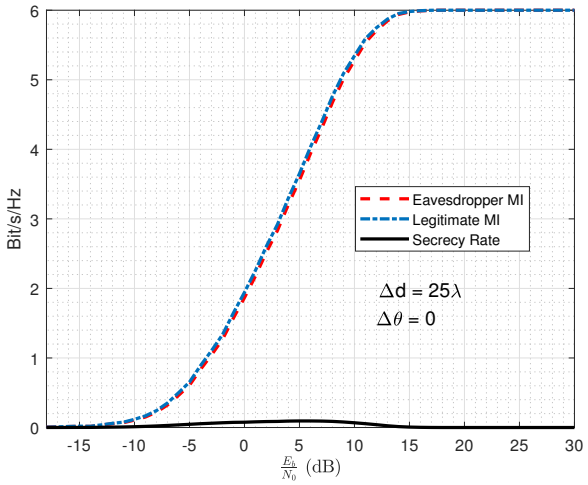

Figure 4. Mutual information associated with the legitimate user and eavesdropper when both users are in the far field and the corresponding secrecy rate.

Let us now consider a scenario where both users are at the same propagation distance to the ULA $d_l = d_m = d_{FA}$ (i.e., $\Delta d = 0°$), but located at different directions. Figure 5 presents the MI and SR considering a scenario where $\theta_m = \theta_l = 0°$ with $\Delta\theta = \theta_l = 5°$.

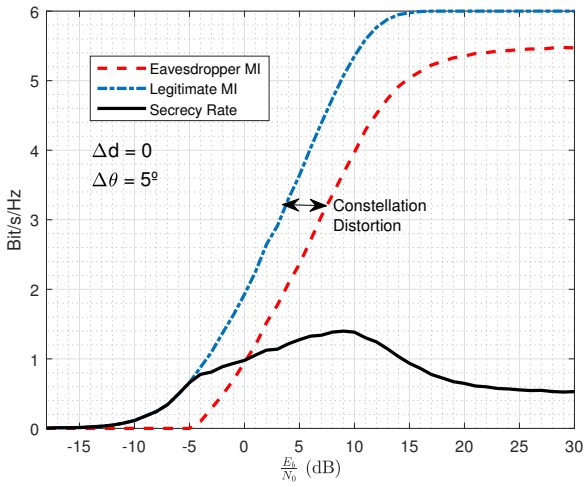

Figure 5. Mutual information associated with the legitimate user and eavesdropper when both users are in the far field with $\Delta\theta = 5°$ and the corresponding secrecy rate.

From the figure, it can be noted there is a horizontal shift in the MI of the eavesdropper, which is explained by its different angular location to the legitimate user. This leads to an increase in the SR, which is due to the distortion associated with the received constellation of the malicious user. This distortion effect is shown in Figure 6, which shows the constellation received by the malicious eavesdropper overlapped with a standard 64-QAM constellation.

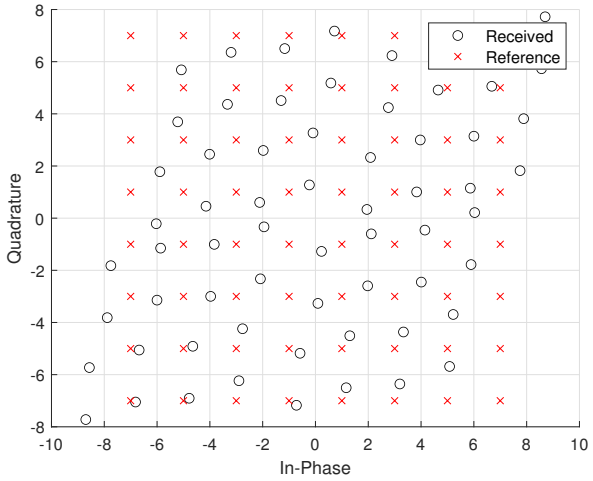

Figure 6. I-Q diagram of the 64-QAM constellation received by the eavesdropper when $\Delta\theta = 5°$.

Figure 7 presents the MI and SR in a scenario where both users are located in the far field ($d_l = d_m = d_{FA}$), with $\Delta d = 0$, $\theta_l = 0°$ and $\Delta\theta = \theta_m = 10°$.

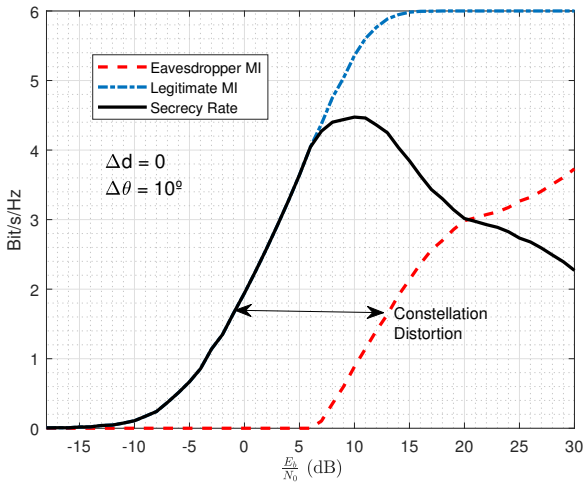

Figure 7. Achievable SR of a malicious eavesdropper and legitimate user. MI between the legitimate user and the eavesdropper. Both users positioned in the far field with $\Delta\theta = 10°$.

From the figure, it can be observed that the eavesdropper's MI does not align with that of the legitimate user, consequently leading to an enhancement in the SR. This shift in MI can once again be attributed to constellation distortion in the far field, given that the normalized beamforming gain is reasonably the same for both users' directions. As a result, it can be noted that PLS can only be obtained in scenarios where the directivity of the transmission is explored (i.e., when users are misaligned).

3.2. Transmission with ELAAs

Aiming to explore the focusing effect available in the near-field region, we propose the use of an ELAA to transmit the different BPSK components. More concretely, we investigate the transmission of a 64-QAM signal subdivided into $K = \log_2(64) = 6$ BPSK components. By following the array geometry described in Section 2.1, we considered that each BPSK signal is transmitted by a given sub-array of the ELAA. Each sub-array has $Q = 180$ antennas (resulting from $P = 5$ and $N = 30^2$) and employs MF beamforming to optimize the signal transmission for the legitimate user.

To evaluate the PLS features of this technique, let us start by defining the received signal as

$$\tilde{s}_n = \sum_{k=1}^{K} \left(\sum_{q=1}^{Q} w_q^{(k)} h_q^{(k)} s_n^{(k)} \right), \tag{11}$$

where $h_q^{(k)}$ is the channel response of the qth antenna of the kth sub-array and $w_q^{(k)}$ is the corresponding beamforming weight used in that antenna (see Equation (4)).

In the following, we present a set of results regarding the MI and the SR. Figure 8 shows the MI and SR considering that both users are at the boresight (with $\theta_m = \theta_l = 0°$ with $\Delta\theta = 0°$) and in the near field of the ELAA (with $d_l = d_{FA}/30$ and $d_m = d + \Delta d$ with $\Delta d = 25\lambda$).

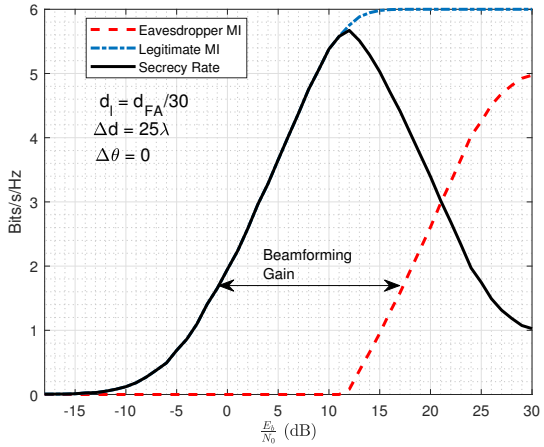

Figure 8. Mutual information associated with the legitimate user and eavesdropper when both users are in the near field.

As it can be analyzed from the figure and in contrast with was observed in Figure 4, we have a clear growth in SR together with the legitimate user's MI. This showcases the focusing effects in the near field since the malicious user no longer experiences maximum beamforming gain at $d_m = d_{FA} + 25\lambda$. In fact, the SR gain can be attributed solely to the normalized beamforming gain disparity between both users' locations, as the constellation received by both is not distorted but only attenuated. This constellation attenuation can be seen in Figure 9, which shows the constellation received by the malicious eavesdropper, overlapped with a standard 64-QAM constellation. This is the case because of the lower normalized beamforming gain attained at a distance $d_m = d + \Delta d$ with $\Delta d = 25\lambda$.

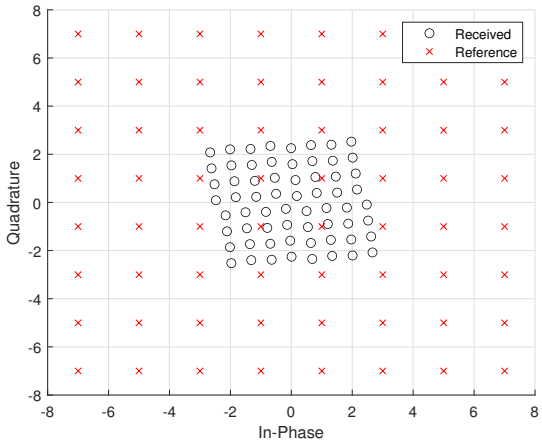

Figure 9. I-Q diagram of the 64-QAM constellation received by the eavesdropper when $\Delta d = 25\lambda$ in the near field.

In Figure 10, a near-field scenario is considered where the focal point remains unchanged, but the eavesdropper is now situated 25λ in front of the legitimate user. As it can be seen from the figure, a parallel analysis to the preceding figure reveals that the SR closely aligns with the MI of legitimate users. Furthermore, it can be observed that the eavesdropper MI remains null. This can be explained due to the sharp nature of the focal point in the near field.

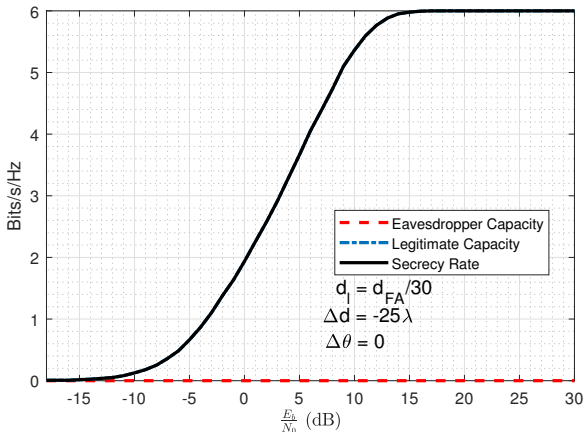

Figure 10. Mutual information associated with the legitimate user and eavesdropper when both users are in the near field.

From Figure 11 a scenario where the eavesdropper is positioned at an angle relative to the legitimate user.

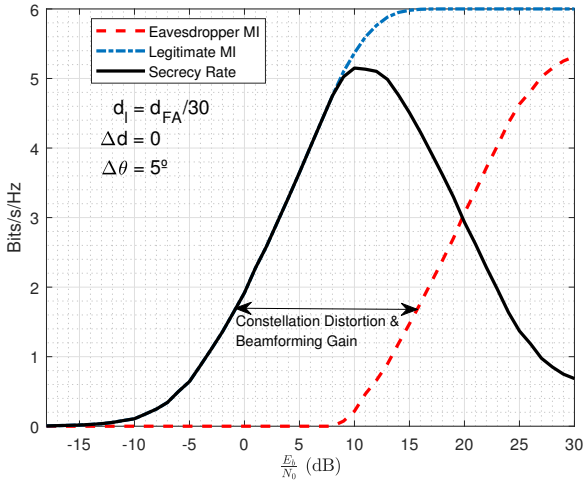

Figure 11. Mutual information associated to the legitimate user and eavesdropper when both users are in the near field with $\Delta\theta = 5$.

The figure depicts a similar scenario to the one presented in Figure 5, where both users are in the near field. Here, both users are at a distance $d_l = d_m = d_{FA}/30$, with $\Delta d = 0$ and $\Delta\theta = 5$. As can be observed and contrary to what happens in the far field, a more significant growth in SR can be attributed not only to a smaller beamwidth in the near field compared to the far-field counterpart but also a distortion in the received constellation due to the angle deviation [17].

4. Conclusions

In this work, we consider the transmission of multilevel QAM constellations with ELAAs. We consider a decomposition scheme to transmit the QAM symbols using highly efficient PAs and study the PLS benefits of such a scheme in terms of MI and SR. It was seen

that in boresight in the far field there was no PLS gain. Moreover, it is shown that PLS can be obtained in the far field thanks to the spatial selectivity in the angular domain. Additionally, it is shown that in the near field, the PLS of the QAM constellation decomposition scheme can be even better since one can take advantage of the beamfocusing effect.

Author Contributions: Conceptualization, P.M. and R.D.; methodology, J.G.; software, J.F.; validation, J.F., J.G. and R.D.; formal analysis, J.F., P.M., J.G. and R.D.; investigation, J.F. and J.G.; writing—original draft preparation, J.F.; writing—review and editing, J.F. and J.G; visualization, P.M. and R.D.; supervision, J.G., P.M. and R.D; All authors have read and agreed to the published version of the manuscript.

Funding: This work is supported by Fundação para a Ciência e a Tecnologia (FCT) and Instituto de Telecomunicações (IT) under projects CELL-LESS6G 2022.08786.PTDC and UIDB/50008/2020.

Data Availability Statement: Data supporting this study are included within the article.

Conflicts of Interest: The authors declare no conflict of interest. The funders had no role in the design of the study; in the collection, analyses, or interpretation of data; in the writing of the manuscript; or in the decision to publish the results.

References

1. Massey, J.L. An introduction to contemporary cryptology. *Proc. IEEE* **1988**, *76*, 533–549. [CrossRef]
2. Bloch, M.; Barros, J.; Rodrigues, M.R.D.; McLaughlin, S.W. Wireless information-theoretic security. *IEEE Trans. Inf. Theory* **2008**, *54*, 2515–2534. [CrossRef]
3. Shiu, Y.S.; Chang, S.Y.; Wu, H.C.; Huang, S.C.H.; Chen, H.H. Physical layer security in wireless networks: A tutorial. *IEEE Wirel. Commun.* **2011**, *18*, 66–74. [CrossRef]
4. Harrison, W.K.; Almeida, J.; Bloch, M.R.; McLaughlin, S.W.; Barros, J. Coding for secrecy: An overview of error-control coding techniques for physical-layer security. *IEEE Signal Process. Mag.* **2013**, *30*, 41–50. [CrossRef]
5. Molisch, A.F.; Ratnam, V.V.; Han, S.; Li, Z.; Nguyen, S.L.H.; Li, L.; Haneda, K. Hybrid beamforming for massive MIMO: A survey. *IEEE Commun. Mag.* **2017**, *55*, 134–141. [CrossRef]
6. Mucchi, L.; Jayousi, S.; Caputo, S.; Panayirci, E.; Shahabuddin, S.; Bechtold, J.; Morales, I.; Stoica, R.A.; Abreu, G.; Haas, H. Physical-layer security in 6G networks. *IEEE Open J. Commun. Soc.* **2021**, *2*, 1901–1914. [CrossRef]
7. Lu, H.; Zeng, Y. Communicating with extremely large-scale array/surface: Unified modeling and performance analysis. *IEEE Trans. Wirel. Commun.* **2021**, *21*, 4039–4053. [CrossRef]
8. Björnson, E.; Demir, Ö.; Sanguinetti, L. A primer on near field beamforming for arrays and reconfigurable intelligent surfaces. In Proceedings of the 2021 55th Asilomar Conference on Signals and Computers, Pacific Grove, CA, USA, 31 October–3 November 2021.
9. Zhang, H.; Shlezinger, N.; Guidi, F.; Dardari, D.; Imani, M.; Eldar, Y. Beam focusing for multi-user MIMO communications with dynamic metasurface antennas. In Proceedings of the 2021 IEEE International Conference on Acoustics, Speech and Signal Processing (ICASSP), Toronto, ON, Canada, 6–11 June 2021.
10. Zhang, H.; Shlezinger, N.; Guidi, F.; Dardari, D.; Imani, M.; Eldar, Y. Beam focusing for near-field multiuser MIMO communications. *IEEE Trans. Wirel. Commun.* **2022**, *21*, 7476–7490. [CrossRef]
11. Ferreira, J.; Guerreiro, J.; Dinis, R. Physical Layer Security with Near-field Beamforming. *IEEE Access* **2023**, *12*, 4801–4811. [CrossRef]
12. Ferreira, J.; Guerreiro, J.; Dinis, R.; Silva, M. On the Jamming Rejection Features of Near-field Beamforming. In Proceedings of the 2023 IEEE 97th Vehicular Technology Conference (VTC2023-Spring), Florence, Italy, 20–23 June 2023; pp. 1–5.
13. Zhang, Z.; Liu, Y.; Wang, Z.-J.; Mu, X.; Chen, J. Physical layer security in near-field communications: What will be changed? *arXiv* **2023**, arXiv:2302.04189.
14. Joung, J.; Ho, C.K.; Sun, S. Spectral Efficiency and Energy Efficiency of OFDM Systems: Impact of Power Amplifiers and Countermeasures. *IEEE J. Sel. Areas Commun.* **2014**, *32*, 208–220 [CrossRef]
15. Astucia, V.; Montezuma, P.; Dinis, R.; Beko, M. On the use of multiple grossly nonlinear amplifiers for highly efficient linear amplification of multilevel constellations. In Proceedings of the 2013 IEEE 78th Vehicular Technology Conference (VTC Fall), Las Vegas, NV, USA, 2–5 September 2013; pp. 1–5.
16. Montezuma, P.; Dinis, R. Multi Antenna Transmission Technique with Constellation Shaping for Secrecy at Physical Layer. In Proceedings of the 2015 IEEE 82nd Vehicular Technology Conference (VTC2015-Fall), Boston, MA, USA, 6–9 September 2015; pp. 1–5.
17. Montezuma, P.; Dinis, R. Implementing physical layer security using transmitters with constellation shaping. In Proceedings of the 2015 24th International Conference on Computer Communication and Networks (ICCCN), Las Vegas, NV, USA, 3–6 August 2015; pp. 1–4.
18. Kapetanovic, D.; Zheng, G.; Russek, F. Physical layer security for massive MIMO: An overview on passive eavesdropping and active attacks. *IEEE Commun. Mag.* **2015**, *53*, 21–27. [CrossRef]

19. Choi, E.; Oh, M.; Choi, J.; Park, J.; Lee, N.; Al-Dhahir, N. Joint precoding and artificial noise design for MU-MIMO wiretap channels. *IEEE Trans. Commun.* **2023**, *71*, 1564–1578. [CrossRef]
20. Alhakami, W.; El-Sayed, H.; Faragallah, O.; El-Mashed, M. Efficient security architecture for physical layer in mmWave communication systems. *IEEE Access* **2022**, *10*, 113923–113934. [CrossRef]
21. Jyothsna, S.; Theagarajan, L. Improving MIMO secrecy rate through efficient power allocation. In Proceedings of the 2022 IEEE 96th Vehicular Technology Conference (VTC2022-Fall), London, UK, 26–29 September 2022.
22. Anaya-López, G.; González-Coma, J.; López-Martínez, F. Spatial degrees of freedom for physical layer security in XL-MIMO. In Proceedings of the 2022 IEEE 95th Vehicular Technology Conference: (VTC2022-Spring), Helsinki, Finland, 19–22 June 2022.
23. Svensson, T.; Eriksson, T. On Power Amplifier Efficiency with Modulated Signals. In Proceedings of the 2010 IEEE 71st Vehicular Technology Conference, Taipei, Taiwan, 16–19 May 2010.
24. Montezuma, P.; Astucia, V.; Dinis, R.; Beko, M. On the Use of Multiple Amplifiers and Antennas for Efficient Directive Transmission with Large Constellations. In Proceedings of the MILCOM 2013–2013 IEEE Military Communications Conference, San Diego, CA, USA, 18–20 November 2013; pp. 1597–1603.